Activation Barrier Scaling for the Spontaneous Evaporation of Confined Water†

Alenka Luzar*

Department of Chemistry, Virginia Commonwealth University, Richmond, Virginia 23284-2006

Received: July 2, 2004; In Final Form: August 12, 2004

We use Glauber dynamics Monte Carlo simulations and umbrella sampling techniques of a lattice gas model for confined water to validate the continuum estimates for the scaling of the activation barrier for evaporation with intersurface separation and barrier dependence on surface composition. Although thermal fluctuations significantly reduce the absolute values of activation barriers, ΔG^*, we find a scaling exponent ($\nu = 1.9 \pm 0.1$) that agrees within statistical limits with the saddle-point approximation, $\Delta G^* \propto D^2$. Devising a method to measure a microscopic analogue of the contact angle θ from simulations, we find good agreement with the continuum prediction, $\Delta G^* \propto 1/\cos\theta$. Combining the known result for the magnitude of the activation barrier and the evaporation rate of molecular water in a specified molecular confinement (Leung, K.; Luzar, A.; Bratko, D. *Phys. Rev. Lett.* **2003**, *90*, 065502-1) with the present scaling results allows us to predict the kinetic viability of the expulsion of water over a range of length scales and between arbitrary physically and chemically modified hydrophobic surfaces characterized by contact angles above 90°.

I. Introduction

When liquid is confined between weakly attractive lyophobic surfaces characterized with contact angles above 90° and the confining distance is sufficiently small, it should spontaneously evaporate.[1] The evaporation transition of a confined liquid and its possible consequence for the attractive force have been noted for some time.[2−6] In these papers, it has been suggested that the primary driving force toward the assembly of large hydrophobic surfaces is associated with evaporation induced by apolar confinement. The issues of the spontaneous evaporation of water between mesoscopic hydrophobic surfaces thus pertain to problems of adhesion and the formation of self-assembly.[1]

Spontaneous evaporation is controlled by competition between bulk energetics (that favors the liquid phase) and surface energetics (that favors the vapor phase). This liquid-to-vapor transition occurs when the grand potential of the confined liquid and confined vapor are comparable:[5]

$$\Omega_l \approx -PV + 2A_w\gamma_{wl} = \Omega_v \approx -P_vV + 2A_w\gamma_{wv} + A\gamma \quad (1)$$

where $V \simeq A_wD$ is the volume of the confined region, $A_w \propto L^2$ is the area of the wall, and $A \propto LD$ is the area of the liquid/vapor interface. The $A\gamma$ term is relevant because of finite lateral size. For an incompressible fluid, the difference in the bulk pressure, P, and the pressure of the coexisting vapor, P_v, is approximated by $\rho\Delta\mu$[7] (where ρ is the number density of the liquid and $\Delta\mu$ is the difference in the chemical potential of bulk liquid from the value at liquid−gas coexistence).

From the above equality, we derived[5] the general expression for the critical threshold distance for the spontaneous expulsion of a liquid confined between surfaces of finite lateral size, L:

$$D_c \cong \frac{2\Delta\gamma}{\rho\Delta\mu + (b\gamma/L)} \quad (2)$$

where

$$\Delta\gamma \equiv \gamma_{wl} - \gamma_{wv} = -\gamma\cos\theta \quad (3)$$

is the Young equation[1] relating the difference in wall/vapor and wall/liquid surface tension to the surface tension of the free liquid−vapor interface, γ, and the contact angle θ. b is a geometry-dependent constant on the order of unity. Equation 2 shows that for (laterally) small confinements the critical separation approaches the confinement lateral size, $D_c = O(L)$. Recently, others have used an analogous equation (eq 2) to study the dewetting-induced collapse of ellipsoidal hydrophobic particles.[8] For macroscopic surfaces, $L \to \infty$, eq 2 reduces to the well-known Kelvin equation, $D \approx 2\Delta\gamma/\rho\Delta\mu$.[9] Dzubiella and Hansen[10] discussed a different generalization of Kelvin equation that incorporates the effect of the electric field, which in addition to the PV term tends to suppress water expulsion. Their extended expression enables studies of phase instability between charged particles such as ionic colloids.

Macroscopic thermodynamics thus predicts that when we have two nonpolar surfaces immersed in a liquid and bring them closer together at a critical distance D_c, liquid will be replaced by vapor, and this effect is shown schematically in Figure 1 (solid curve). If we plot the density in the confinement, ρ_D, going from large to small surface separation, then the density drops from liquid to vapor density at a critical distance D_c given by eq 2.

For water confined between hydrocarbon surfaces (characterized by a contact angle of ~110°[1]) and at ambient conditions, this transition is predicted to occur at a threshold separation on the order of 10^2 nm. However, this large distance, predicted by thermodynamics, is not supported by experiments that directly measure forces between hydrocarbon surfaces immersed in water.[11] Such experiments detect liquid water at much smaller separations, well below D_c. Indeed, cavitation phenomena have been observed only at or close to contact with the surface force

† Part of the special issue "Frank H. Stillinger Festschrift".

* E-mail: aluzar@vcu.edu.

10.1021/jp0470703 CCC: $27.50
Published on Web 10/22/2004

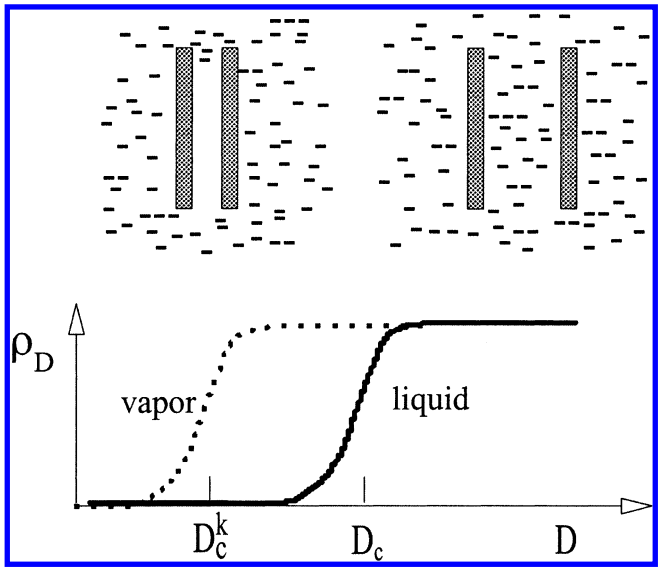

Figure 1. Fluid density ρ_D vs intersurface separation D. This schematic profiles reflect the stable liquid confined between two lyophobic surfaces on the right and the stable vapor on the left. D_c and D_c^k denote thermodynamic and kinetic threshold, respectively, for the spontaneous evaporation of a confined liquid that is metastable in between.

apparatus (SFA) where the refractive index measurements allow the unambiguous detection of vapor between the surfaces.[11] In other cases, cavitation or the presence of vapor can often be inferred although there is sometimes considerable uncertainty in the correct interpretation of the experimentally determined force curves.[11] It follows that the force between hydrophobic surfaces is, strictly speaking, often measured under nonequilibrium conditions.[11]

The above experimental findings suggest that higher density persists at much smaller separations than predicted by thermodynamics (dotted curve in Figure 1). Thus, in addition to the equilibrium threshold separation, D_c, the kinetic threshold separation, D_c^k, comes into play. Liquid water in this regime (between D_c and D_c^k, Figure 1) is metastable.[12]

The reason for metastability is a considerable activation barrier for confinement-induced evaporation.[13−16] Such activation barriers are inaccessible to direct measurements. There have been recent attempts to deduce activation barriers indirectly for capillary evaporation from measurements at high pressure.[17] The elevated pressure P_{in} was applied to push water into mesoporous hydrophobic material to determine the extrusion pressure, $P_{ex} < P_{in}$, under which evaporation from the pores becomes kinetically viable. Such an experiment works for conditions where evaporation is rapid and pressure is required to prevent it. Using a mean-field model that incorporated a negative line-tension term, the authors were able to obtain barrier heights and extrusion pressures consistent with their experiment.[17]

In silico experiments (i.e., computer simulations) are well suited to address the problem of when spontaneous evaporation is kinetically viable under ambient conditions. There were previous attempts to study water in narrow hydrophobic confinements by open-ensemble molecular simulations[2,8,15,18−24] capable of capturing capillary evaporation and equilibrium with the bulk water phase. Although metastable liquid phases observed in some of these studies highlighted the importance of kinetic barriers between liquid and vapor phases, few of them elucidated dynamic aspects of confinement-induced evaporation.[5,7,14−16,25−30]

Molecular dynamics simulations to study evaporation are still limited to surface separations too small to determine the kinetic threshold distance, D_c^k (Figure 1). Specialized simulation algorithms such as the use of the gliding-plane boundary conditions[23,31] may accelerate the kinetics artificially to allow the system thermodynamics to be studied more efficiently. Facilitated evaporation obtained by such a technique at a water film thickness of ∼5 nm[23] is, however, not indicative of real evaporation kinetics that would be attainable by molecular dynamics.

The computational strategy we adopt to answer the question of when the expulsion of water from hydrophobic confinement is viable at all length scales and at different surface compositions is as follows. First, we do a molecular simulation at a plate separation D of several molecular diameters and a specified molecular confinement to determine the activation barrier height and nucleation rate. Next, we use a coarse-grained description of the liquid to assess the scaling of barrier height with surface separation, D, and with varying contact angle θ. In our simulations, we consider model surfaces with contact angles ranging from those characteristic of hydrocarbons and fluorocarbons (∼110°)[1] to rain-repellant coatings (∼160°).[33] Numerical prediction regarding the nucleation times at larger separations should provide pertinent information for distances that can be considered in surface force apparatus (SFA) measurements. Until recently, such measurements have not been possible below ∼5 nm. SFA experiments using the high-speed camera to test for time-dependent effects such as microcavity formation during hydrophobic interaction are underway.[32]

In our recent work,[16] we reported the first explicit computation of ΔG^* and the absolute rate of water evaporation from hydrocarbon-like confinement using atomistic simulations. The advent of high-speed computers and the development of new algorithms[25] enabled us to determine the magnitude of the barrier and kinetics of the drying transition events. We used a combination of grand canonical Monte Carlo (GCMC) and molecular dynamics (MD) to compute the free-energy barrier for forming a vapor tube bridging between the two surfaces and the rates of emptying a hydrocarbon-like pore using a reactive flux formalism.[34,35] We considered surface separations of about four molecular diameters (1.4 nm), the width shown to exceed the limit of mechanical instability (spinodal) for a given range of surface−water interaction strength.[15,36] For water film four molecular diameters thick, we found an activation barrier of $\sim 18.7 k_B T$ and a vapor nucleation rate of the order of 10^5 nm^2 s^{-1}. As a consequence, we found a rapid expulsion of water from a narrow (∼1 nm) confinement, taking about 10 μs to see one evaporation event per nanometer-sized area. Extending the simulations to length scales accessible to experiments (e.g., SFA) requires a larger interplate separation to be considered, and we have to rely on coarse-grained modeling.

We reported on using the newly developed umbrella sampling/Monte Carlo algorithms[25] in conjunction with a coarse-grained model of confined aqueous systems[14] that enable systematic studies of activation barriers for capillary evaporation at increased surface separations. We demonstrated that fluctuations in the shape of the vapor pocket/tube significantly reduced the activation free energy of tube formation.[25] This result highlighted the limitations of the saddle-point approximation,[13,37,38] which calculates activation free energies by considering a single transition-state geometry.

The interesting question remains of whether shape fluctuations reflect on the scaling of the activation barrier for vapor tube formation with surface separation as well. Continuum theories predict that ΔG^* grows approximately as γD^2.[13,37] The deviation of the scaling exponent from 2 could also indicate that there

are other factors in addition to surface work. For example, in their recent study, Lefevre et al.[17] showed that nucleation energetics may involve a contribution to $\Delta\Omega$ proportional to separation D. Depending on its magnitude, the presence of a line-tension[40] term linear in D may be reflected in the nonquadratic scaling of ΔG^* with D. It is important to learn the conditions under which a single term will dominate the scaling of the activation barrier with surface separation D. Another interesting question is concerned with the dependence of the barrier on surface hydrophobicity and with the validity of an approximate analytic relation between the barrier height and contact angle of confining surfaces.[42]

To answer these questions, in the present work we extended the previous method[25] that allows us to compute the vapor tube formation free-energy barrier at larger intersurface separations and smaller values of contact angles. We use Glauber dynamics Monte Carlo[41] simulations for a lattice gas, whose parameters are tuned to the thermodynamic properties of water.[14]

On the basis of simulation results, we find that whereas fluctuations in the shape of the vapor pocket lower ΔG^* at larger surface separation the scaling exponent is not visibly affected. Thermal fluctuations seem to reduce interfacial free energy for all shapes and sizes similarly. Furthermore, we confirmed that for the range of contact angles we considered the activation barriers vary with the contact angle in close agreement with the prediction of a simple mean-field approximation.[42]

II. Simulation Details

A. Model. The confined liquid is modeled by a 3D lattice gas on a cubic lattice of size $L \times L \times D$. The nearest-neighbor lattice gas Hamiltonian is given by

$$H = -\epsilon \sum_{\langle ij \rangle} n_i n_j - \sum_{i \in \text{surface}} \epsilon_i^s n_i - \mu \sum_i n_i \qquad (4)$$

where $n_i = 0, 1$ represents vapor/liquidlike sites. The lattice gas parameters, specifically, the nearest-neighbor interaction ϵ, the chemical potential μ, and the lattice spacing a, are chosen to match the surface tension and isothermal compressibility of water at ambient conditions ($T = 298$ K and $P = 1$ atm). Model parameters that reproduce desired properties are estimated[14] by employing the quasi-chemical (mean-field) approximation due to Guggenheim:[43,44] $a = 0.193$ nm, $\epsilon \approx 2a^2\gamma = 1.2646 k_B T$, and $\mu = -6\epsilon/2 + 1.84247 \times 10^{-4} k_B T$.

We vary the surface field ϵ_i^s from 10 to 35% of the bulk field ϵ to mimic water next to ideal, virtually repulsive walls or an oily surface. The surface size effect is taken into account by varying the lateral surface size, L, from 64 to 256 in units of lattice spacing.

Periodic boundary conditions are applied in the lateral directions (x, y). The confined liquid is thus bounded by a liquid layer outside the simulation box and is at equilibrium with a bulk reservoir at a given temperature T and chemical potential μ. According to this choice, the surfaces are finite objects immersed in bulk liquid, as in an experimental/natural setting. The Metropolis sampling scheme is used in all Monte Carlo runs.[45] An accelerated Monte Carlo scheme[46] has also been attempted. However, at our temperature (far away from the critical temperature of the lattice gas) and in our slablike geometry, it is found that this algorithm does not lead to an appreciable increase in simulation speed.

B. Activation Barriers. We have successfully developed a constrained umbrella sampling technique to compute ΔG^* to evaporation in a confined fluid.[25] We have chosen the size of the vapor pocket, N_c, in the middle of the liquid layer as the reaction coordinate and have imposed various constraints to facilitate the sampling of our metastable system. For all technical details, the reader is referred to ref 25. A vapor tube imposes a geometric constraint in which a continuous path of vapor must exist to connect the two surfaces. ΔG for a vapor tube of a certain size (the omission of the asterisk means that the tube is not necessarily at the transition state) is referenced to the metastable confined liquid layer without tubes penetrating it. The topologies of the reference and final states are therefore different. To apply umbrella sampling, we used a forward−backward sampling scheme to interpolate between the two states. In the process, we found that the thermal fluctuations were important and that not imposing the geometric constraint associated with a vapor tube actually decreased ΔG^* because of tunneling.[49]

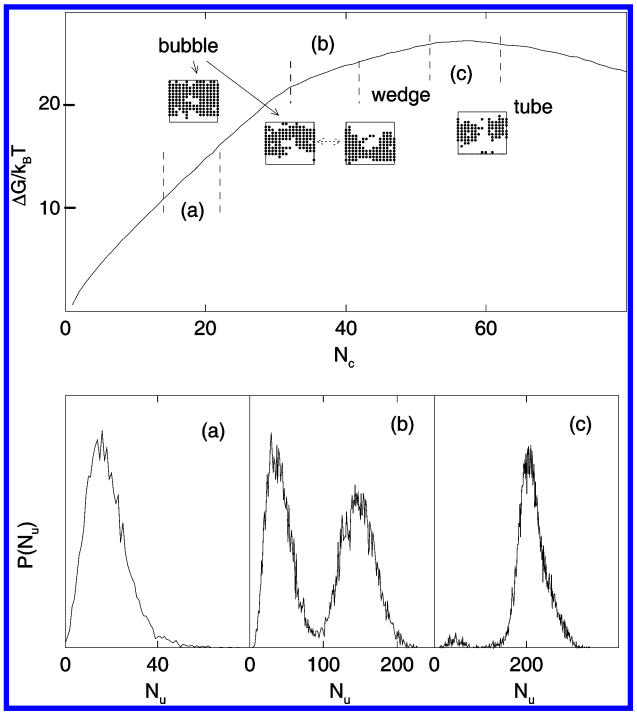

Figure 2. Spontaneous vapor pocket shape transformations for $D/a = 14$, where a is the lattice spacing of molecular size along the reaction coordinate N_c, the size of the vapor pocket. (Top) (a−c) umbrella sampling windows used to calculate the free-energy profile, $\Delta G/k_BT$. For $D/a > 14$, transformations are no longer spontaneous, and umbrella sampling (or multicanonical sampling) for N_u, the number of empty lattice sites above or below the vapor pocket, within each window is required. (Bottom) probability distributions of N_u for (a) bubble, (b) wedge, and (c) tube vapor pocket geometries.

Our choice of the reaction coordinate is equivalent to the one traditionally used in studying nucleation (vapor-to-liquid transition). The validity of this choice in the present case (liquid-to-vapor transition) was discussed in the previous work[25] and has further been confirmed by recent simulations performed on the small system size of Lennard-Jones particles using transition-path sampling.[50] The dynamical path-sampling methods[47,48] determine (rather than assume) the reaction coordinate but are too costly to apply to the large lattice gas systems of interest. Furthermore, our atomistic simulations on a smaller system reveal[16] a diffusive barrier crossing[51] of the liquid-to-vapor transition, a situation that poses additional restrictions for using such methods.[52]

It turns out that our umbrella sampling method[25] is adequate for D up to ∼16 solvent layers (depending on the magnitude of

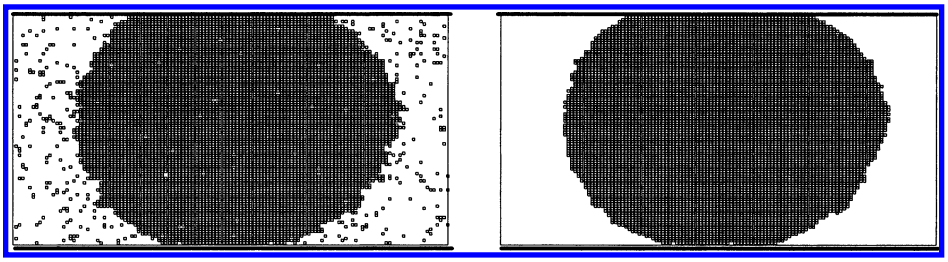

Figure 3. Geometrical construction used to estimate the apparent contact angle θ at each surface−liquid attraction, ϵ_s, from simulation using mass-conserving dynamics for a liquid droplet between two adjacent surfaces. (Left) cross section of a liquid droplet between surfaces before averaging. (Right) cross section of a liquid droplet between surfaces with in-plane averaging.

surface−liquid attraction, ϵ_s). In this regime, spontaneous shape fluctuations suffice for the size-induced transformation between the bubble, wedge (pocket penetrating one liquid−vapor interface), and tube (pocket penetrating both interfaces) geometries (Figure 2). However, to investigate barrier scaling with D, especially for $D > 16$ solvent layers, and higher values of liquid−surface attraction, an additional problem is encountered: our simulations at D exceeding ~16 reveal the presence of a few distinct low-energy domains in configuration space (for a fixed pocket size). These domains are separated by increasingly unfavorable regions that prevent the ergodic sampling of pocket geometries. The problem of efficiently sampling the shape fluctuations is circumvented by using a second series of umbrella samplings within each vapor pocket size window. The coordinate of the second umbrella sampling is the number of empty lattice sites above and below the vapor pocket, N_u (Figure 2). By computing the free-energy profiles as a function of this localized number of empty sites, the relative contributions of the bubble, wedge, and tube geometries to each vapor pocket size window are determined.

This is a computationally expensive route. To alleviate computational costs, we considered a variation of multicanonical sampling by artificially reducing the barriers between geometric transformations (i.e., different favorable pocket geometries) according to the algorithm of Besold et al.[53] The method involves the use of shape functions, which are added to the model Hamiltonian to level out the free-energy barriers between favorable geometries. We add to our usual lattice gas Hamiltonian (eq 4) a shape function, $f(N_u, N_c)$ with $H_{eff} = H + f(N_u, N_c)$. This proved to be sufficient because our calculations indicate two shape transitions (bubble to wedge and wedge to tube) that turned out to be sequential (Figure 2).

C. Contact Angle Estimates. We need to connect the microscopic interaction parameter ϵ_s with an observable measure of surface/liquid interfacial free energy. Thus, at each surface−liquid attraction we explicitly compute the apparent contact angle θ for a liquid droplet between two adjacent surfaces (Figure 3) using mass-conserving dynamics. We obtain a smooth liquid−vapor interface by averaging over the lattice gas configurations over 50 000 passes and over the dimension perpendicular to the interface (z). The simulation cell for computing the contact angle is periodic in the x and y directions and is confined by two walls and $z = D + 1$ (with the lattice spacing used as the unit of length). In view of the discrete (on-lattice) representation we use, the contact angle θ (i.e., the angle between the droplet/vapor interface and the wall at the wall surface) is approximated by $\theta \cong \arccos(\Delta/\sqrt{(\Delta^2 + 1)})$, where Δ denotes the average difference between lateral positions of the droplet/vapor interface (relative to the droplet center) in the second and first layers of the interfacial liquid (i.e., for $z = 1$ and $z = 2$ or for $z = D - 1$ and $z = D$). For $\Delta = 0$, the contact angle is 90°. For $\Delta = \infty$, it is either 0 or 180°.

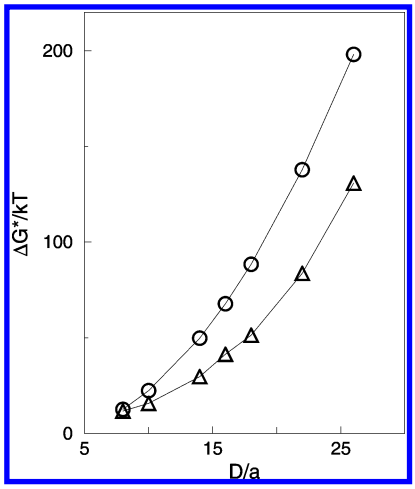

Figure 4. Activation barriers as functions of the distance between extended hydrophobic surfaces ($L = 64$, $\epsilon_s = 0.1\epsilon$) in units of lattice spacing, a, for saddle-point estimates (○), $\Delta G^* \propto (D - 2\bar{l})^2$, where $\bar{l}$ is the mean vapor film thickness, and umbrella sampling calculations (△). Note that even at these virtually repulsive hydrophobic surfaces and $P = 1$ atm, the vapor film that develops next to surfaces with average thickness $\bar{l}$ is less than about one lattice spacing (one solvent layer) thick.[14,56,57]

The geometry and proper averaging allow for the extraction of θ as a function of ϵ_s, but large values of contact angles ($\theta >$ 150°) are harder to determine accurately. The difficult part is the defining of the mean interface position. Some averaging has to be performed; otherwise, for each configuration, the fluctuations are too large to define a meaningful interface. We average over 10 or 20 slabs in the y direction for each pass. A majority sum rule is used. If more than 50% of the slabs under averaging contain a liquid particle at a particular x position, then that position is considered to be liquidlike. Otherwise, it is vaporlike. This averaging distance does not strongly affect the results except in cases of large contact angles. In those cases where the mean occupation number at the wall−liquid interface is $\langle n \rangle < 0.5$, averaging over a large enough number of slabs along the y direction will eventually make all sites vaporlike because of the majority rule. In these cases, the results are somewhat dependent on the averaging method.

III. Results and Discussion

A. Activation Barriers: Magnitudes. Figure 4 represents the simulated ΔG^* under the constraint of a fixed lateral position of the cavity center of mass for $L = 64$ and $\epsilon_s = 0.1\epsilon$ (10% hydrophilicity). We compare activation barriers for evaporation as a function of intersurface separation obtained via umbrella sampling/MC calculations, ΔG^*_{MC}, with those estimated from the saddle-point approximation, ΔG^*_{MF}.[37] A regime at which the saddle-point estimate is easily obtained in the form of a closed expression is one for very high contact angles where

surfaces are shielded by a thin vaporlike film of average thickness $\bar{l}$.[54] The geometry of a vapor tube is an hourglass-like object narrow at the waist that widens into cones that merge with the vapor films adjacent to the surfaces.[5,37] For such cases of virtually repulsive surfaces where $\cos\theta \approx -1$, the activation barrier for vapor tube formation is approximated by $\Delta G^* = \pi\gamma(D - 2\bar{l})^2/6$.[37] In the case of weakly attractive hydrophobic surfaces that we simulated and at ambient presure, $\bar{l}$ is around one solvent layer,[14] in qualitative agreement with other theoretical work[55,57] as well as some experiments.[56] Using the simulation value for $\bar{l}$,[14] the continuum theory[37] consistently exceeds the simulation results (Figure 4). The absolute difference between the results of the two methods increases with the interplate separation, which will result in a huge underestimation of evaporation rates predicted by the mean-field theory at large D. At first, these results seem counterintuitive because one would expect continuum theory to perform better at larger length scales. However, as D is increased, there are more possibilities for how the vapor tube really forms. In other words, the effect of fluctuations in the shape of the vapor pocket/tube increases with interplate separation. Contrary to the assumption in all continuum estimates of the tube-formation free energy, it is not necessary to have unity probability of tube formation at all times. The shape fluctuations of a vapor tube help reduce the free energy of vapor tube formation. Results presented in Figure 4 demonstrate the importance of fluctuations in the shape of the vapor pocket/tube, the reduction in the free energy of tube formation increasing roughly in proportion with the magnitude of the barrier.

B. Activation Barriers: Scaling with Intersurface Separation. The difference $\Delta G^*_{MF} - \Delta G^*_{MC} = \Delta\,\Delta G^*_{fl}$, where $\Delta\,\Delta G^*_{fl}$ accounts for fluctuations in the shape of the vapor pocket, increases with the size of the tube (Figure 4). Our simulations are intended to show whether these fluctuations reflect on the scaling of the activation barrier for tube formation and if so, how much.

When simulation is used to study the barrier scaling with D, we need to ascertain that our results correspond to the asymptotic limit of large L, where $D \ll L$, and the scaling exponent is independent of L. Because possible L dependence is most pronounced for surfaces with the highest contact angles, we present a comparison of two sets of results, one for $L/a = 64$ and one for $L/a = 128$, at $\epsilon_s = 0.1\epsilon$, the most hydrophobic surfaces we considered. Because of unfavorable surface−liquid interaction, these surfaces are separated from the liquid by a thin vapor layer.[5,6,14,54,58] The effect of L on ΔG^* stems from the variation of the capillary wave amplitude corresponding to the fluctuation of the vapor/liquid interface that varies with surface size approximately as $L \ln L$.[39] A wider vapor film results in a smaller distance that the vapor tube has to bridge to initiate the evaporation process, thus lowering ΔG^*. This is exactly what our previous simulations[14,25] have shown. ΔG^* becomes less dependent on L when surfaces become more hydrophilic (stronger surface−liquid attraction) because hydrophilicity suppresses the formation of the surface vapor film.[59,60] On the basis of small differences between the curves for $L/a = 64$ and 128, shown in Figure 5, it is clear that the size $L/a = 256$ we use in the remaining, less hydrophobic cases is sufficient to secure asymptotic (large L) behavior.

As discussed above, in evaluating the results presented in Figure 5, the thickness of the interfacial vapor film, $\bar{l}$ of approximately one solvent layer, cannot be neglected, and scaling of ΔG^* with $(D - 2\bar{l})$, not only D, applies.[37] The usual

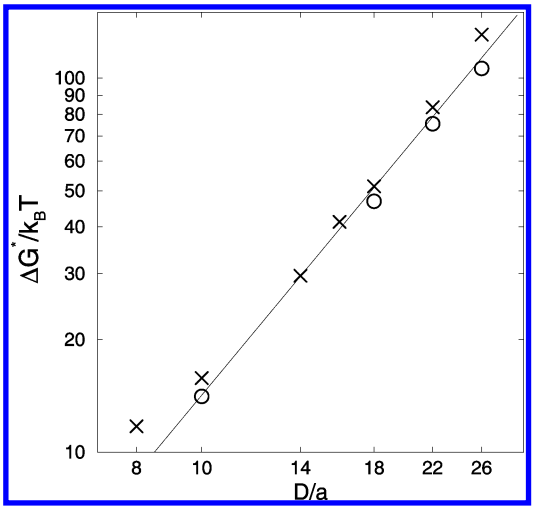

Figure 5. Scaling of activation barriers for vapor tube formation with intersurface separation at different lateral sizes of surfaces, L, in units of lattice spacing $a = 0.193$ nm and liquid−surface attraction $\epsilon_s = 0.1\epsilon$. ×, $L/a = 64$, slope ≈ 2.3. ○, $L/a = 128$, slope ≈ 2.1. Note that with these virtually repulsive hydrophobic surfaces true scaling applies to $D - 2\bar{l}$ and not to D alone.[37] Taking into account the values of $\bar{l}$ from ref 14 brings the scaling exponents down from 2.3 and 2.1 to 2.1 and 2.0.

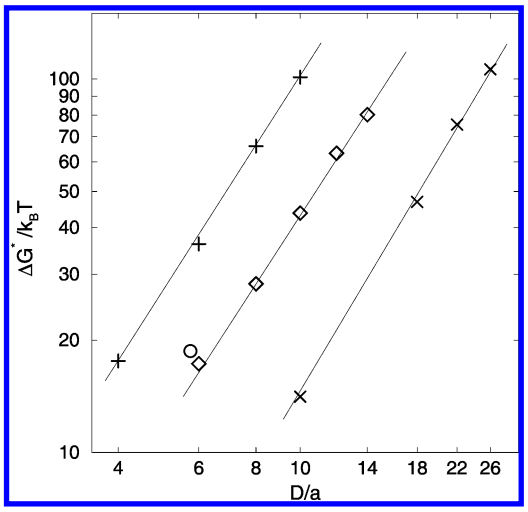

Figure 6. Scaling of activation barriers for vapor tube formation with intersurface separation with varying liquid−surface attraction, ϵ_s, that progressively gives lower contact angles, θ. ×, $L/a = 128$, $\epsilon_s = 0.1\epsilon$, $\theta \approx 165°$, slope ≈ 2.1. ◇, $L/a = 256$, $\epsilon_s = 0.2\epsilon$, $\theta \approx 136°$, slope ≈ 1.9. +, $L/a = 256$, $\epsilon_s = 0.35\epsilon$, $\theta \approx 109°$, slope ≈ 1.9. ○, SPC[63] water for infinite plate geometry and for simulated contact angle $\theta \approx 135 \pm 5$ taken from ref 16 for comparison.

mean-field scaling of $\Delta G^* \approx D^2$ is recovered for large enough D, when $D \gg 2\bar{l}$.

In Figure 6, we present the scaling of the activation barrier at different values of hydrophilicity (surface−water attraction) of confining surfaces from 20 to 35%. The corresponding contact angles obtained from simulation are ∼135 and ∼109° (see the next section); the curve with 10% attraction and an estimated contact angle of ∼165° for $L/a = 128$ from Figure 5 is included for comparison. In all cases, we observe activation barrier scaling very close to that predicted by the saddle-point approximation,[13] $\Delta G^* \propto D^2$. These results suggest $\Delta\Delta G^*_{fl}$ to be approximately proportional to the area of the vapor tube and hence D^2 such that the shape fluctuations reduce ΔG^* without affecting the scaling exponent. It is not clear if small but consistent deviations from exponent 2 reflect numerical uncertainties or are related to shape fluctuations and other effects

TABLE 1: Contact Angles θ for Surfaces with Different Water/Surface Interactions ϵ_s[a,b]

ϵ_s/ϵ	θ_{MC}	θ_Y
0.1	165 ± 10	143
0.2	136 ± 5	127
0.35	109 ± 5	107.5

[a] Given as fractions of water/water contact energy, ϵ. [b] Subscripts MC and Y denote the Monte Carlo simulation results and predictions from the Young equation, respectively.

such as the line-tension work,[17,61] and dependence of interfacial tension described by the Tolman length.[54]

Our results indicate that the surface tension term strongly dominates other possible contributions to ΔG^*. A recent study by Lefevre et al.[17] highlighted the importance of the line-tension term, but this contribution is most important for objects comparable to molecular size. The same authors[17] discuss the role of the pressure (PV) term, which is important at high P. At extreme pressure, this term could lead to cubic scaling of ΔG^* with D. For the largest critical vapor cavity we considered (i.e., for $D/a = 10$ and $\epsilon_s = 0.35\epsilon$), we estimated the PV^* term to be $\sim 0.85 k_B T$, and the activation barrier for such a case is $\sim 100 k_B T$ (Figure 6). Therefore, we conclude that at ambient conditions in which we are interested, the PV term cannot be significant.

In Figure 6, we also compare the estimated activation barriers from a coarse-grained model of water to those for molecular water[62] confined between hydrocarbon plates[15,63,64] (contact angle $\sim 135° \pm 5$)[16] at a molecular-scale thickness of the confined water slab of 1.1 nm that we used in our previous work.[16] We find satisfactory agreement (circle in Figure 6). This result looks promising for using a coarse-grained description of a molecular solvent confined between detailed surfaces, including biological ones.[65] Such studies can provide the first insight into whether cooperative hydrophobic dewetting between model hydrocarbon surfaces plays any role in protein aggregation and folding, for example.[8] The few available all-atom molecular dynamics simulations concerned with this phenomenon in biological systems seem to be contradictory.[66−68]

Discussions of confinement-induced evaporation require one to make an important distinction between different criteria used to characterize hydrophobicity. For cavitation in any system to take place, the contact angle must be above 90°. When only short-range interactions are present, this requirement is equivalent to having the ratio of the surface/water and water/water attraction, ϵ_s/ϵ, below 0.5. In the literature, a less stringent or weaker condition of hydrophobicity for surfaces to attract water less than water attracts itself is often invoked.[69,70] This condition suffices to promote hydrophobic association but not for capillary evaporation. Note that it would be very hard to identify a biological surface to fulfill the first criterion, but there are an abundance of surfaces that fulfill the second one. For sure, the molecular roughness[71] and hydrophobic/hydrophilic heterogeneity[14] and electrostatic effects[10,68] add to the complexity of the problem.

C. Role of the Contact Angle. The values for θ obtained with the method described in section IIC are listed in Table 1. The method we use is similar in spirit to the one proposed by Hautman and Klein.[72] These authors developed an elegant approach to estimate microscopic analogues of contact angles via molecular dynamics simulations. It is interesting that both calculations—the present one on the coarse-grained level and the one by Hautman and Klein on the molecular level[72]—consistently overestimate the contact angles' values based on experiments for water/hydrocarbon surfaces[1] by about 20%. Our earlier molecular simulation[16] using the identical water potential as that in ref 72 and coarse-grained hydrocarbon Lennard-Jones-like interactions also yielded a contact angle that was ~20% higher than expected. In the case of molecular simulations, it has been suggested[72] that the discrepancy might be due to highly idealized hydrophobic surfaces in both papers. Real hydrocarbon chains are polar and polarizable, and including such effects into the model would likely decrease the calculated angles in both cases.[72] Taking into account other work[62,73] suggests that an important source of discrepancy might be due to line tension, with positive line tension[73] making contact angles larger.

In Table 1, we compare apparent contact angles from our simulations with the ones predicted using the Young relation (eq 3), along with the assumption that $\gamma \approx \epsilon/2a^2$: $-\cos\theta = 1 - (2\epsilon_s/\epsilon)$. Note the satisfactory agreement at small contact angle values, but a greater deviation is apparent at higher values. This observation would be consistent with smaller statistical accuracy at large θ. However, virtually repulsive surfaces characterized by high contact angles (in our case 165°) face vaporlike dewetting layers (films).[5,6,55,59] In this case, thermal fluctuations are particularly important because of capillary-wavelike fluctuations,[5] and the geometric construction used in the calculation of contact angles becomes rather vague.

A comparison of scaling curves for different contact angles reveals virtually identical scaling at all values of θ (Figure 6). For this to be possible, activation barriers should vary with the contact angle in a consistent way, independently of intersurface separation D.

For small pressures such as the ambient pressure $P \approx 1$ atm and neglecting the shape variation with θ, ΔG^* is expected to vary as $\sim \gamma D^2/\cos\theta$.[42] Our results for activation barriers at contact angles of $\theta = 109$ and 135° are in excellent agreement with this prediction (Table 2). The ratios of calculated barriers at the two contact angles for $D/a = 6$, 8, or 10 fall within ±5% of the theoretical prediction, $\Delta G^*(D, 109°)/\Delta G^*(D, 136°) = \cos(136°)/\cos(109°) = 2.21$ (Table 2). The presence of vapor films that develop at extremely hydrophobic model surfaces (e.g., the model case with $\epsilon_s = 0.1\ \epsilon$, $\theta = 165°$ and shown in Figures 5,6) preclude the use of the above relationship at such artificial conditions unless the reduction in the liquid layer thickness is taken into account. Upon inclusion of this effect, the barrier change associated with the increase in θ from 136 to 165° conforms to predicted scaling with $\cos\theta$.[42] Note that this scaling is within ±5% of the theoretical prediction only when contact angles are calculated by considering thermal fluctuations.

TABLE 2: Activation Barriers for Evaporation at Surface Separations $D = 6$, 8, or 10 Lattice Spacings and Contact Angles Obtained from Monte Carlo Simulations, $\theta_{MC} = 136$ or 109°[a]

D/a	$\Delta G^*(D, 136°)/k_BT$	$\Delta G^*(D, 109°)/k_BT$	$\Delta G^*(D, 109°)/\Delta G^*(D, 136°)$	$\Delta G^*(D, 109°)\cos(109°)/\Delta G^*(D, 136°)\cos(136°)$
6	17.3 ± 0.4	36.2 ± 0.6	2.09	0.95
8	28.4 ± 0.8	66 ± 1	2.32	1.05
10	44 ± 1	102 ± 1.5	2.32	1.05

[a] At all distances, the ratio of the barriers for the two contact angles agrees within 5% with the approximate mean-field prediction,[41] $\Delta G^* \approx 1/\cos\theta$.

Extrapolation from intermediate to lower contact angles (closer to 90°) enables us to estimate ΔG^* at conditions where critical cavity sizes and barrier magnitudes make simulations impractical even within the coarse-grained model we use. This regime is important because low contact angles slightly above 90° are characteristic of many hydrophobic surfaces observed in nature. If the relation $\Delta G^* \approx 1/\cos\theta$[42] is approximately valid, then reducing the contact angle from say 110 to 100° nearly doubles the barrier to evaporation. In view of barrier values for $\theta = 109°$ presented in Figure 6, it is clear that in most naturally occurring systems we cannot expect to observe spontaneous evaporation except from molecular-sized confinement.

IV. Conclusions

We find that the nucleation barrier for water evaporation increases with the confinement width with apparent scaling exponent $\nu = 1.9 \pm 0.1$. Within numerical uncertainty, it is close to the exponent predicted from the saddle-point approximation.[13] Fluctuations in the shape of the vapor pocket are found to reduce the absolute values of activation barriers significantly. These fluctuations might also have some effect on the scaling exponent. However, any systematic deviations from mean-field scaling exponent 2 are too small to be distinguished from the numerical inaccuracy of the method. Simplified models for the grand potential Ω also consider the existence of terms with a linear, quadratic, and cubic dependence on intersurface separation D.[17] These terms are associated with line and surface tension and pressure work, respectively. Obviously, the scaling cannot exactly apply unless one term is dominant. We find that for low pressures such as ambient pressure studied here, only the surface term can significantly exceed all others.

The rapid scaling of the activation barrier implies that in many practical situations in nature the height of the activation barrier for evaporation can lead to a strong metastability of the confined liquid phase. It also implies that hydrophobic interaction can be under kinetic, in addition to thermodynamic, control. The results shed light on the inability of equilibrium arguments to explain force measurements with SFA for strongly hydrophobic surfaces immersed in water. As is often the case, the results mean that it will be very difficult to prove experimentally that water expulsion occurs as two hydrophobic surfaces come together.[74] When detected so far,[11] cavitation/evaporation occurs only very, very close to contact, and any experimentally observed long-range attraction is likely due to other phenomena.

In agreement with the mean-field prediction,[42] we find that the results for the nucleation barrier between specified surfaces can be used to estimate the barrier for confinement with arbitrary contact angles, $\theta > 90°$. Important surface characteristics ignored in our present study are surface roughness and possible nonuniform composition because ideally smooth and uniform surfaces are rarely found in biology or in practical materials. Depending on the pattern of hydrophilic patch distribution on hydrophobic surfaces, we have shown that a small change in surface composition can have a strong effect on the dynamics of capillary drying.[14] Furthermore, hydrophobic properties can be significantly enhanced by increasing the roughness of the surface. Superhydrophobic surfaces, characterized by contact angles above 150°, require both appropriate surface roughness and low surface energy. Fractal structures have been reported to effectively enhance the hydrophobicity of a solid surface.[75] Although the consequences of macroscopic roughness are rather well understood,[76,77] less is known about roughness effects on molecular and mesoscopic levels. It appears likely that the line-tension effect can be significantly enhanced with increasing molecular-scale roughness of the material. One of the consequences would be a change in the scaling of the activation barrier to evaporation, a question we will address in future work.

Acknowledgment. I am grateful for invaluable help and discussions with Kevin Leung in contributing to the project. I thank Dusan Bratko for his critical reading of the manuscript. I acknowledge Gary Grest for the contact angle issues. This work was supported by the National Science Foundation (CHE-0211626) and the National Center for Supercomputing Applications (CHE-010023N).

References and Notes

(1) Israelachvili, J. N. *Intermolecular and Surface Forces*; Academic Press: London, 1992.
(2) Luzar, A.; Bratko, D.; Blum, L. *J. Phys. Chem.* **1987**, *86*, 2955.
(3) Berard, D. R.; Attard, P.; Patey, G. N. *J. Chem. Phys.* **1993**, 98, 7236.
(4) Patey, G. N. *Ber. Busen-Ges. Phys. Chem.* **1996**, *100*, 885.
(5) Lum, K.; Luzar, A. *Phys. Rev. E* **1997**, *56*, R6283.
(6) Lum, K.; Chandler, D.; Weeks, J. D. *J. Phys. Chem. B* **1999**, *103*, 4570.
(7) MacDowell, L. G. *J. Chem. Phys.* **2003**, *119*, 453.
(8) Huang, X.; Margulis, C. J.; Berne, B. J. *Proc. Nat. Acad. Sci. U.S.A.* **2003**, *100*, 11953.
(9) Evans, R. *J. Phys.: Condens. Matter* **1990**, *2*, 8989.
(10) Dzubiella, J.; Hansen, J. P. *J. Chem. Phys.* **2003**, *119*, 12049.
(11) For the latest review on direct measurements of the forces between hydrophobic surfaces in water, see Christenson, H. K.; Cleasson, P. M. *Adv. Colloid Interface Sci.* **2001**, *91*, 391.
(12) Debenedetti, P. G. *Metastable Liquids: Concepts and Principles*; Princeton University Press: Princeton, NJ, 1996.
(13) Yuschencko, V. S.; Yaminsky, V. V.; Shchukin, E. D. *J. Colloid. Interface Sci.* **1983**, *96*, 307.
(14) Luzar, A.; Leung, K. *J. Chem. Phys.* **2000**, *113*, 5836.
(15) Bratko, D.; Curtis, R. A.; Blanch, H. W.; Prausnitz, J. M. *J. Chem. Phys.* **2001**, *115*, 3873.
(16) Leung, K.; Luzar, A.; Bratko, D. *Phys. Rev. Lett.* **2003**, *90*, 065502-1.
(17) Lefevre, B.; Saugey, A.; Barrat, J. L.; Bocquet, L.; Chanlaix, E.; Gobin, P. F.; Vigier, G. *J. Chem. Phys.* **2004**, *120*, 4927.
(18) Wallqvist, A.; Berne, B. J. *J. Phys. Chem.* **1995**, *99*, 2893.
(19) Brovchenko, I. V.; Geiger, A.; Paschek, D. *Fluid Phase Equilib.* **2001**, *183*, 331.
(20) Forsman, J.; Jonsson, B.; Woodward, C. E.; Wennerstrom, H. *J. Phys. Chem. B* **1997**, *101*, 4253.
(21) Spohr, E.; Trokhymchuk, A.; Henderson, D. *J. Electroanal. Chem.* **1998**, *450*, 281.
(22) Brodskaya, E. N.; Zakharov, V. V.; Laaksonen, A. *Langmuir* **2001**, *17*, 4443.
(23) Hayashi, T.; Pertsin, A. J.; Grunze, M. *J. Chem. Phys.* **2002**, *117*, 6271.
(24) Jensen, M. O.; Mouritsen, O. G.; Peters, G. H. *J. Chem. Phys.* **2002**, *120*, 9729.
(25) Leung, K.; Luzar, A. *J. Chem. Phys.* **2000**, *113*, 5845.
(26) Hummer, G.; Rasaiah, J. C.; Noworyta, J. P. *Nature* **2001**, *414*, 188.
(27) Becksetin, O.; Sansom, M. S. P. *Proc. Natl. Acad. Sci. U.S.A.* **2003**, *100*, 7063.
(28) Karla, A.; Garde, S.; Hummer, G. *Proc. Natl. Acad. Sci. U.S.A.* **2003**, *100*, 10175.
(29) Truskett, T. M. *Proc. Natl. Acad. Sci. U.S.A.* **2003**, *100*, 10139.
(30) Anishkin, A.; Sukharev, S. *Biophys. J.* **2004**, *86*, 2883.
(31) Pertsin, A. J. Private communication.
(32) Israelachvili, J. Private communication.
(33) Shibuichi, O. T.; Satoh, N.; Tsujii, K. *J. Phys. Chem.* **1996**, *100*, 19512.
(34) Bennett C. H. In *Algorithms for Chemical Computations*; Christofferson, R. E., Ed.; American Chemical Society: Washington, DC, 1977; p 63. Chandler, D. *J. Chem. Phys.* **1978**, *68*, 2959.
(35) Hynes, J. T. In *Solvent Effects and Chemical Reactivity*; Tapia, O., Bertran, J., Eds.; Understanding Chemical Reactivity Series, Vol. 17, Kluwer: Dordrecht, The Netherlands, 1996.
(36) Truskett, T. M.; Debenedetti, P. G.; Torquato, S. *J. Chem. Phys.* **2001**, *114*, 2401.
(37) Lum, K.; Chandler, D. *Int. J. Thermophys.* **1998**, *19*, 845.
(38) Restagno, F.; Bocquet, L.; Biben, T.; Charlaix, E. *J. Phys.: Condens. Matter* **2000**, *20*, A419.

(39) Weeks, J. D. *J. Chem. Phys.* **1977**, *67*, 3106.
(40) Rowlinson, J. S.; Widom, B. *Molecular Theory of Capillarity*; Oxford University Press: New York, 1989.
(41) Glauber, R. *J. Math. Phys.* **1963**, *4*, 294.
(42) Yaminsky, V. V.; Ohnishi, S.; Ninham, B. In *Handbook of Surfaces and Interfaces of Materials*; Nalwa, H. S., Ed.; Academic Press: New York, 2001; Vol. 4.
(43) Guggenhein, E. A. *Mixtures*; Oxford University Press: New York, 1952. Guggenhein, E. A. *Proc. R. Soc. London, Ser. A* **1994**, *183*, 213.
(44) Pendzig, P.; Dieterich, W.; Nitzan, A. *J. Chem. Phys.* **1997**, *106*, 3703.
(45) Metropolis, N.; Rosenbluth, A. W.; Rosenbluth, M. N.; Teller, A. H.; Teller, E. *J. Chem. Phys.* **1953**, *21*, 1087.
(46) Bortz, A. B.; Kalos, M. H.; Lebowitz, J. L. *J. Comput. Phys.* **1975**, *17*, 10.
(47) Dellago, C.; Bolhuis, P. G.; Chandler, D. *J. Chem. Phys.* **1998**, *108*, 9236.
(48) Zuckerman, D. M.; Woolf, T. B. *J. Chem. Phys.* **1999**, *111*, 9475.
(49) We found a loose analogy of our transition-state barrier compared the classical case. In our case, the fluctuations in the local liquid−vapor interface play the role of "tunnelling", allowing the tube constraint to be bypassed along the reaction coordinate, thus lowering ΔG^*.
(50) Bolhuis, P. G.; Chandler, D. *J. Chem. Phys.* **2000**, *113*, 8154.
(51) ten Wolde, P. R.; Ruiz-Montero, M. J.; Frenkel, D. *J. Chem. Phys.* **1999**, *100*, 1591.
(52) Bolhuis, P. G. *J. Phys.: Condens. Matt.* **2033**, *12*, S113.
(53) Besold, G.; Risbo, J.; Mouritsen, O. G. *Comput. Mater. Sci.* **1999**, *15*, 311.
(54) Stillinger, F. H. *J. Solution Chem.* **1973**, *2*, 141.
(55) McCormick, T. A. *Phys. Rev. E* **2003**, *68*, 061601.
(56) Jensen, T. R.; Jensen, M. O.; Reitzel, N.; Balashev, K.; Peters, G. H.; Kjaer, K.; Bjornholm, T. *Phys. Rev. Lett.* **2003**, *90*, 086101.
(57) Mamatkulow, S. I.; Khabibullaev, P. K.; Netz, R. R. *Langmuir* **2004**, *20*, 4756.
(58) Hummer, G.; Garde, S. *Phys. Rev. Lett.* **1998**, *80*, 4193.
(59) Wallqvist, A.; Gallicchio, E.; Levy, R. M. *J. Phys. Chem. B* **2001**, *105*, 6745.
(60) Ashbaugh, H. S.; Paulaitis, M. E. *J. Am. Chem. Soc.* **2001**, *123*, 10721.
(61) Oxtoby, D. W.; Talanquer, V. *J. Chem. Phys.* **2001**, *14*, 2793.
(62) Berendsen, H. J. C.; Postma, J. P. M.; van Gunsetern, W. F.; Hermans, J. In *Intermolecular Forces*; Pullman, B., Ed.; Reidel: Dordrecht, The Netherlands, 1981.
(63) Lee, C. J.; McCammon, J. A.; Rossky, P. J. *J. Chem. Phys.* **1984**, *80*, 4448.
(64) Sheely, J. C.; Patey, G. N. *Mol. Phys.* **1996**, *88*, 385.
(65) ten Wolde, P. R.; Chandler, D. *Proc. Natl. Acad. Sci. U.S.A.* **2002**, *99*, 6539.
(66) Rhee, Y. M.; Sorin, E. J.; Jayachandran, G.; Lindahl, E.; Pande, V. S. *Proc. Natl. Acad. Sci. U.S.A.* **2004**, *101*, 6456.
(67) Huang, Q.; Ding, S.; Hua, C. Y.; Yang, H. C.; Chen, C. L. *J. Chem. Phys.* **2004**, *121*, 1969.
(68) Zhou, R.; Huang, X.; Margulis, J. C.; Berne, B. J. *Science* **2004**, *305*, 1605.
(69) Leckband, D.; Israelachvili, J. *Q. Rev. Biophys.* **2001**, *34*, 105.
(70) Dill, K. A.; Bromberg, S. *Molecular Driving Forces*; Garland Science: New York, 2003.
(71) Cheng, Y. K.; Rossky, P. J. *Nature* **1998**, *392*, 696.
(72) Hautman, J.; Klein, M. L. *Phys. Rev. Lett.* **1991**, *67*, 1763. Mar, W.; Hautman, J.; Klein, M. L. *Comput. Mater. Sci.* **1995**, *3*, 481.
(73) Werder, T.; Walther, J. H.; Jaffe, R. L.; Halicioglu, T.; Koumoutsakos, P. *J. Phys. Chem. B* **2003**, *107*, 1345.
(74) Christenson, H. K. Private communication.
(75) Erbil, H. Y.; Demirel, A. L.; Avci, Y.; Mert, O. *Science* **2003**, *299*, 1337.
(76) Wenzel, R. N. *Ind. Eng. Chem.* **1936**, *28*, 988.
(77) Marmur, A. *Langmuir* **2004**, *20*, 3517.